Behavior of Cold Bend Pipes under Bending Loads

M. Sen[1]; J. J. R. Cheng[2]; and J. Zhou[3]

Abstract: Ground movement along a buried pipeline often places the line in net compression. The local buckling resistance at cold bends is less than at straight sections, and hence, local buckling tends to occur at bends. Correspondingly, this full-scale testing program was conducted to investigate the local and global load-deformation relationships for seven cold bend pipes under applied loads. The specimens were loaded under bending, axial load, and internal pressure until local buckling occurred, and their curvatures were subsequently increased to establish their postbuckling behaviors. It was demonstrated though these tests that the buckling strain of the cold bend pipes was considerably lower than a straight pipe and that the presence of internal pressure exhibited a predominant role on the specimens load-deformation behaviors. It was also established that the behavior of the specimens was relatively unaffected by the bending methods that were employed during cold bending. **DOI: 10.1061/(ASCE)ST.1943-541X.0000219.** © *2011 American Society of Civil Engineers.*

CE Database subject headings: Pipes; Bending; Buckling; Imperfections; Strain.

Author keywords: Pipe; Cold bend; Bending; Buckle; Strain; Imperfection.

Introduction

Cold bends are frequently required along pipeline routes where there are severe changes in the slope of the trench (vertical bend), or at locations where an abrupt change in the horizontal orientation of the pipeline (horizontal bend) is required. These pipelines may encounter sizeable applied deformations that are caused from thermal loads, soil liquefaction during an earthquake, or from soil movement along unstable slopes. When assessing the effects of geotechnical movements on a line in service, traditional engineering practice is partially based on the judgment that the geotechnical movements tend to concentrate pipe deformations in the vicinity of bends, as shown in Fig. 1. Consequently, it is of interest to understand the conditions that contribute to local buckling in cold bends, and the conditions that contribute to the amplification of local buckles in the bends into "wrinkles" in which significant plastic deformations and cross sectional distortions accumulate. It is critical to prevent the development of these wrinkles because they may initiate a rupture in the pipeline, which would cause serious safety, environmental, and economical consequences (Bouwkamp et al. 1973). Current pipeline design codes do not provide prediction methods for the determination of the buckling strain for cold bends (ASME 1999); however, it is important to understand the allowable strain that a cold bend can accumulate prior to buckling to ensure adequate maintenance of the pipeline.

This research project was designed to study the behavior of cold bend pipes under combined loading. Specifically, the strain at the onset of local buckling of cold bends was investigated herein. This was primarily accomplished through the full-scale testing of one straight pipe, and seven cold bend pipes that demonstrated varying cross sections, material properties, and bending methods that were employed during cold bending (Sen et al. 2008). To evaluate the load-deformation behavior of the specimens, the pipes were installed into a testing frame and loaded under axial load and in-plane bending. They were also subjected to various internal pressures that were similar to pressures applied in field conditions. During testing the curvatures of the specimens were increased until a local buckle formed, and then further increased to study their postbuckling behaviors. Sufficient instrumentation was installed onto the specimens and test setup to assess both their local and global deformations during testing (Sen et al. 2004).

Test Parameters

The parameters of the specimens were selected to allow for the study of typical cold bends that are used in gas pipelines. The four specimen parameters that were evaluated herein were the pipe: diameter/thickness ratio, material grade, internal pressure, and the kink angle/kink spacing, as described in Table 1. Full-scale specimens were employed to eliminate scale effects.

Previous research has demonstrated that the diameter/thickness ratio is an important parameter in assessing the critical strain for a straight pipe (Dorey et al. 2001), and it is believed that this concept will remain true for a cold bend pipe. Accordingly, the specimens studied herein exhibited diameter/thickness ratios that ranged from 43 to 92. These specimens were comprised of six nominal 30 in. diameter (NPS 30) pipes and two NPS 24 pipes, with varying wall thicknesses.

The materials for the pipe walls were grade X60, X65, and X80, which are common steel grades used for modern pipes. All of these materials exhibited a rounded stress-strain relationship at the yield point, within the bend region of the specimens (Sen et al. 2005a). In contrast to the straight portion for many of the test specimens that exhibited a yield plateau; the rounding of the material stress-strain relationship in the bend regions occurred because of the work hardening that was induced to the pipe wall during the cold bending process (Fukada et al. 2002).

[1]Enbridge Pipelines Inc., 10201 Jasper Avenue, Edmonton, Canada T5J 3N7 (corresponding author). E-mail: millan.sen@enbridge.com

[2]Dept. of Civil and Environmental Engineering, Univ. of Alberta, Edmonton, Canada T6G 2G7.

[3]TransCanada Pipelines Ltd., 450-1st Street S.W., Calgary, Canada T2P 5H1.

Note. This manuscript was submitted on February 1, 2008; approved on March 10, 2010; published online on March 12, 2010. Discussion period open until October 1, 2011; separate discussions must be submitted for individual papers. This paper is part of the ***Journal of Structural Engineering***, Vol. 137, No. 5, May 1, 2011. ©ASCE, ISSN 0733-9445/2011/5-571–578/$25.00.

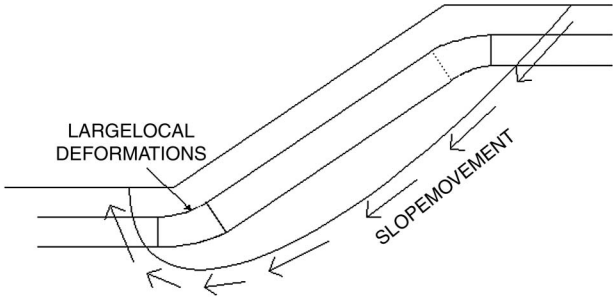

Fig. 1. Response of cold bend to slope movement elevation view

There were three different internal pressures applied to the specimens in the testing program, and each internal pressure was associated with two specimens. These internal pressures caused hoop stresses of 40, 60, and 80% of their yield stresses, and are the maximum internal pressures allowed by the Japanese, Italian, and Canadian Pipeline Codes, respectively. In addition, two of the specimens were loaded without internal pressure, where for each unpressurized specimen there was an identical specimen tested with internal pressure.

The final bend angle of a cold bend pipe is achieved by generating a series of several kinks over regularly spaced intervals, as opposed to a single uniform bend (Fukada et al. 2001). It is more cost efficient to use a larger kink angle with a lower number of kinks during cold bending; however, using a large kink angle may produce detrimental effects on the critical strain of the cold bend. Consequently, the bending method employed during cold bending was investigated. For example, specimens 4 and 5 demonstrated the same central bend angle; however, specimen 4 was kinked 0.5° every 300 mm in length, while specimen 5 was kinked 1.0° every 600 mm in length. The bending method was also the only parameter studied when comparing the behaviors of specimens 6 and 8 during testing, as described in Table 1.

A horizontal length of approximately 7.4 m was maintained for all of the specimens, which ensured that the length/diameter was greater than 10 for all of the specimens. The central bend angles ranged from 9 to 14°, and are bend angles typically employed in field conditions. The average bending degree/diameter ranged from 1.0 to 1.5 for the specimens (0.0017 to 0.0025 degrees/mm length for the NPS 24 specimens, and 0.0013 to 0.0020 degrees/mm length for the NPS 30 specimens. This parameter was governed by the various pipeline codes, where for example the Canadian Pipeline Code CSA Z662 (2003) specified that the maximum allowable bending degree/diameter for a cold bend pipe is 1.5 (CSA 2003).

Experimental Setup and Procedure

Experimental Setup

A self-equilibrating loading frame was constructed to conduct the experimental program. The loading frame consisted of two tension members that were bolted at each end to a bending beam, and the specimens were installed within this rectangular frame as shown in Fig. 2. The specimen was loaded during testing with a hydraulic jack, where the jack load was applied eccentric to the pipe end centerline, as shown in Fig. 3. This hydraulic jack was positioned at the middle of one of the bending beams, and during testing the jack was braced against the bending beam on one end and pushed against a hinge on rollers on its other end. The hinge was connected to the bottom of a beam that was orientated vertically. The vertical

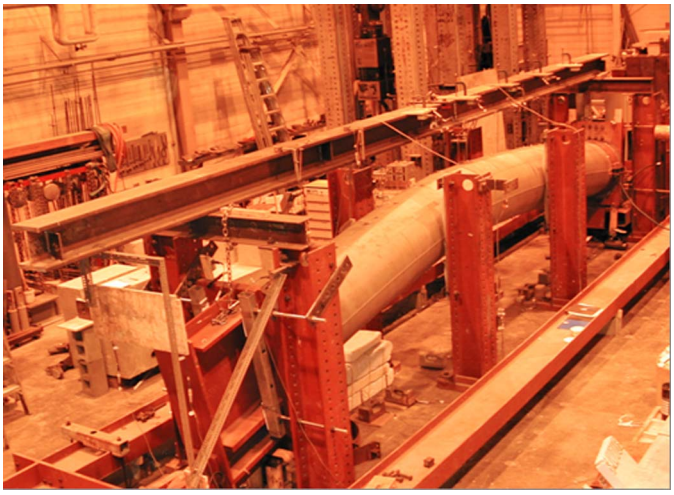

Fig. 2. Overhead of test setup

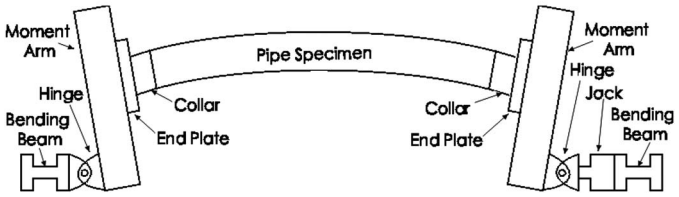

Fig. 3. Schematic of test setup elevation view

Table 1. Measured Specimen Properties

Specimen/ group	Diameter (mm)	Thickness (mm)	Diameter/ thickness	SMYS (MPa)	Bend angle (°)	Bending degree/ diameter	Kink angle/interval[a] (°/mm)	Internal pressure[b] (%SMYS)
1/1	760	11.5	66	414	—	—	0	60
2/1	760	11.6	66	414	11.9	1.4	—	60
3/1	761	11.4	66	414	12.2	1.4	—	0
4/2	608	14.2	43	550	10.1	1.3	0.5/300	40
5/2	608	14.2	43	550	10.2	1.3	1.0/600	40
6/3	762	8.3	92	448	9.4	1.0	0.5/381	80
7/3	760	8.3	92	448	13.7	1.5	0.75/381	0
8/3	761	8.4	92	448	13.2	1.5	0.75/381	80

[a]Kink angle/interval was not measured for specimens 2 and 3.
[b]Hoop stress caused by internal pressure at start of test.

beam was used as a moment arm that provided the 600 mm of eccentricity to the jack load on the specimen. An end plate was bolted to the top of this moment arm, and the specimens were welded to this end plate.

At the nonjack side of the test setup, the pipe was welded to another endplate. This endplate was bolted to a moment arm that was identical to that on the jack side of the loading frame. Near the bottom of the moment arm was a hinge connected to a deep beam. This beam was the bending beam that was attached to the nonjack side end of the tension members.

Considerable bracing was required on the loading frame to ensure that the rotation in the specimen was limited to the applied bending plane. Columns were positioned on each side of the pipe at each of the one-third length locations, to restrain the pipe from movement in the lateral direction during testing. Braces that contacted each of the moment arms at two locations in the vertical directions were used to restrain the specimen from twisting about its longitudinal axis. Finally, vertical bracing was provided at the ends of the testing frame and at the roller location, to resist the upward movement of the frame that would otherwise occur because of the vertical direction friction forces that were released during the rotating of the pins in the hinges. Teflon pads were installed at the contact surface with the pipe for all of the braces to minimize friction forces during testing.

Experimental Procedure

The initial step in testing was to carefully align the specimen within the testing frame, to minimize the out-of-plane moment applied to the pipe during loading. Following this, the ends of the pipe were welded to the end plate on the moment arms using a full penetration groove weld. This ensured that the tensile strength of the connection was greater than that of the pipe. Then the pipes were filled with water, which was necessary because the internal pressure was provided to the pipes through hydraulic pressure.

The first step in the loading of the pipes was to apply the internal pressure. Following this, collars were installed at the ends of the specimen to prevent end buckling. This failure mode was a concern because welding of the pipe generated residual stresses and prevented ovalization at its ends, which caused a stress concentration. End buckling was extremely undesirable because it is caused by the testing setup, and would not occur in cold bends under field conditions. Accordingly, the collars acted to restrain the radial deformation at the ends of the pipe, so that the bending capacity of the ends became greater than that of the middle of the specimen.

After the collars were tightened, the pipe was loaded axially with the hydraulic jack. This applied a bending moment to the pipe equal to the jack load multiplied by its eccentricity to the specimen centerline. For the unpressurized specimens, the jack load also applied axial compression to the pipe. For the pressurized specimens, the jack load reduced the axial tension force in the pipe wall caused by the internal pressure. This axial tension load from the internal pressure was caused by the end plates that were used to contain the water pressure at the ends of the specimen. Thus, when pressurized, the water pressed outward against the end plates, which tended to pull the ends of the specimen apart. The net axial load in the specimens was maximum at the beginning of the test, and continuously reduced until the peak moment was achieved.

The jack load was increased at 100 kN intervals during the elastic phase of testing. After each stoppage in loading, water was drained from the specimen to bring the internal pressure back to the initially prescribed testing pressure. This was necessary because prior to buckling, the containment volume of the pipe decreased from the axial shortening that was caused by the jack load, which acted to increase the internal pressure that was generated from the water inside of the pipe.

After the strains at the ends of the specimen approached the yield strain, action was required to discourage buckling at the ends of the specimen. The first action was to loosen the end collars to allow for the specimen to gradually ovalize over the length of the collars, as opposed to it abruptly ovalizing adjacent to the collars where the pipe was not stiffened. In addition, the lateral braces that were located at the on-third length locations of the specimen, as shown in Fig. 2, were removed. This was necessary because these braces were installed to be snug against each side of the pipe during the initial test setup. Accordingly they acted as stiffeners to the outside of the pipe, because they prevented the radial expansion of the specimen that was necessary for ovalization to occur. Because the moment resistance of an ovalized cross section is less than that of a circular cross section, buckling in the middle section of the pipe was encouraged when it was permitted to ovalize.

Once the peak load was achieved, the loading method was changed to displacement control. That is, the longitudinal movement of the hinge on rollers was monitored, and the specimen was loaded by increasing the jack stroke until the hinge traveled a specified distance. This loading method was necessary because after the peak moment was achieved; when the jack stroke was increased the specimen's load resistance would correspondingly decrease. Additionally, after the specimen buckled the diameter of the pipe at the buckled region increased during loading. This resulted in a greater containment volume for the pipe, which caused a decrease in the internal pressure. Consequently, after buckling occurred the internal pressure was increased to the prescribed testing pressure at each load step. The stroke of the jack was increased until the postbuckling behavior of the specimen was established.

Test Observations

The test observations for the pressurized specimens were similar, so are concurrently discussed. A linear load-deformation relationship was observed at the beginning of these tests. As this relationship became nonlinear, the strains predominantly accumulated toward the ends of the pipes, until end buckle prevention actions were carried out. Following this, the second-order effects from the applied moment at the middle of the pipes encouraged a buckle to form within the middle third of their lengths. The formation of this buckle corresponded to the peak load during testing, which was both preceded and followed by a long period of inelasticity where the slope of the load-deformation relationship of the specimens was nearly zero. The buckle was in the form of an outward bulge-shaped buckle as shown in Fig. 4, which was the typical local failure mode for a pressurized pipe under bending loads (Bouwkamp et al. 1973). Following the peak load, the load capacity of the specimen continually decreased until the jack stroke limit of 300 mm was exhausted.

The test observations for the unpressurized specimens were different from those for the pressurized pipes. During initial loading, considerable ovalization was observed throughout the specimen lengths. This was caused by the inward radial direction component of the pipe wall forces in combination with the absence of the outward acting internal pressure (Boyle et al. 1981). As the load in the pipes approached the peak load, it was observed that several of the initial imperfection ripples commenced to amplify in magnitude, as shown in Fig. 5. As the load further increased, one of the ripples gradually increased in strain more rapidly than the rest of the specimen, and became a buckle, and this buckle was diamond shaped, as illustrated in Fig. 6. Following buckling of the specimen,

Fig. 4. Pressurized specimen bulge-shaped buckle

Fig. 5. Unpressurized specimen ripples before buckling

a sudden reduction in the jack load was observed. This was a result of the sharp decrease in the moment resistance of the pipe cross section at the buckle location (Beer and Johnston et al. 1992). During postbuckling, the load capacity of these specimens decreased more severely than the pressurized specimens.

Test Results

Maximum Moment

The eight test specimens were divided into three groups, with the specimens within each group demonstrating identical cross sectional geometries as shown in Table 1. Correspondingly, the global behaviors of the specimens within Group 1, Group 2, and Group 3 are compared with one another herein. These three groups are composed of specimens 1 to 3, specimens 4 and 5, and specimens 6 to 8, respectively. To assess the peak moment achieved by the specimens during the tests, the interactive plastic moment equation for a straight pipe in Eq. (1) (Mohareb et al. 1994) was calculated for the eight specimens. This equation was employed in this research to calculate the predicted peak moment values in Table 2. This equation neglects the influences of strain hardening, local buckling, or any effects of cold bending.

Fig. 6. Unpressurized specimen diamond-shaped buckle

$$M_P = \cos\left\{\frac{\pi}{2\cdot\sqrt{1-\frac{3}{4}\cdot\left(\frac{\sigma_\theta}{\sigma_y}\right)^2}}\cdot\left(\frac{C}{C_y}-\frac{1}{2}\cdot\frac{\sigma_\theta}{\sigma_y}\right)\right\}\cdot\sqrt{1-\frac{3}{4}\cdot\left(\frac{\sigma_\theta}{\sigma_y}\right)^2}\cdot Z\cdot\sigma_y \quad (1)$$

where Mp = plastic moment capacity; $\sigma\theta$ = circumferential stress; σ_y = yield stress; C = applied axial force; C_y = axial load to cause yield when the pipe is unpressurized; and Z = plastic section modulus.

In Table 2 the test and predicted peak moments were fairly similar for all of the Group 1 specimens. The test moments for specimens 1 and 2 were somewhat greater than the predicted peak moment. Specimen 3 demonstrated a peak moment that was less than that of specimens 1 and 2, but the predicted peak moment was greater for specimen 3 than for specimens 1 and 2. This discrepancy occurred because Eq. (1) neglects any local buckling of the specimen, which demonstrates that the unpressurized specimen buckled prior to full plastification of the pipe cross section. This is further verified in the load-deformation curves described in Figs. 7–9, where the unpressurized specimens exhibit a steep slope immediately prior to the peak moment, which indicates that the pipe materials were close to elastic at the onset of buckling.

The test-to-predicted ratios for the Group 2 specimens were moderately greater than one, which indicates that the specimens achieved their plastic moment capacity prior to buckling. Also, the moment capacity of specimen 5 was similar to that of specimen 4. Based on this information, it may be suggested that the varying kink angles did not significantly affect the moment capacities of these cold bends.

For the Group 3 specimens, the test peak moment for specimen 8 was slightly greater compared with specimen 6, which is contrary to what would be intuitively expected because specimen 8 was cold bent more severely than specimen 6. Moreover, as the peak moments of these two specimens were very similar, this verifies the global results from specimens 4 and 5 where the bending method did not significantly affect the cold bends moment capacities. The moment capacity of specimen 7 was 15% less than that of specimen 8, which verifies the behaviors of specimens 2 and 3 wherein the moment capacity of the unpressurized cold bend was less than that of the similar pressurized cold bend. The test to predicted ratio for specimen 7 was less than one, which verifies the results from specimen 3, where the cold bending process reduced the plastic moment capacity of the unpressurized specimen.

Table 2. Test Prediction and Results Summary

Specimen/ group	Net axial load[a] (%SMYS)	Predicted peak moment (kNm)	Test peak moment (kNm)	Predicted critical strain (%)	Test critical strain (normalized)[c]
1/1	0.3	2,095	2,585	2.04	1.00
2/1	7.4	1,837	2,453	2.07	0.51
3/1	−17.2	2,487	1,982	0.97	0.23
4/2	−0.4	2,650	2,817	2.36	0.60
5/2	−0.4	2,652	2,990	2.35	0.52
6/3	14.9	2,192[b]	1,941	1.72	0.57
7/3	−18.6	2,009	1,727	0.56	0.17
8/3	16.5	2,192[b]	2,028	1.71	0.74

[a]Jack load—pressure force against endplates (−compression), at maximum moment during test.
[b]Predicted maximum moment calculated as the yield stress multiplied by the plastic section modulus because Eq. (1) would not converge for these specimens.
[c]The test critical strain for all of the specimens is normalized against specimen 1.

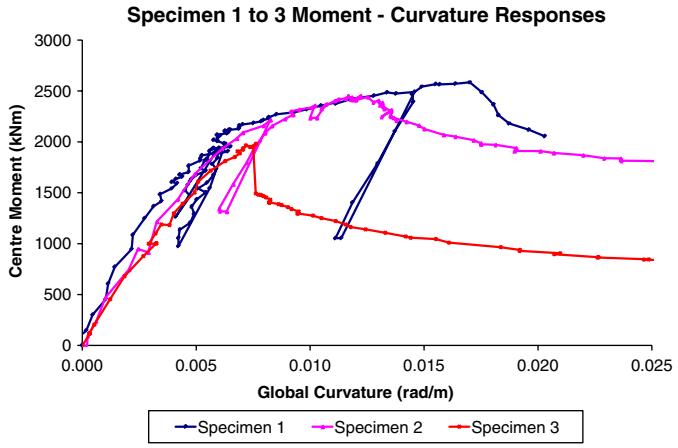

Fig. 7. Group 1 specimens moment-curvature responses

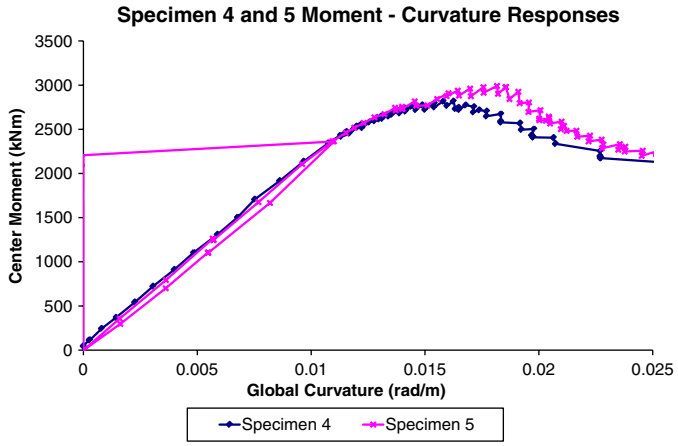

Fig. 8. Group 2 specimens moment-curvature responses

The maximum moments during testing for the pressurized pipes were greatest for the Group 2 specimens, the next greatest were those of the Group 1 specimens, and the peak testing moments for the Group 3 specimens were the lowest of the pressurized specimens. This is a similar order to that predicted using Eq. (1), which demonstrates that the peak moment during the testing of the cold bend pipes were considerably influenced by the plastic section modulus, which is a function of the D/t ratio (Beer and Johnston 1992). For the unpressurized pipes, the peak moment for specimen

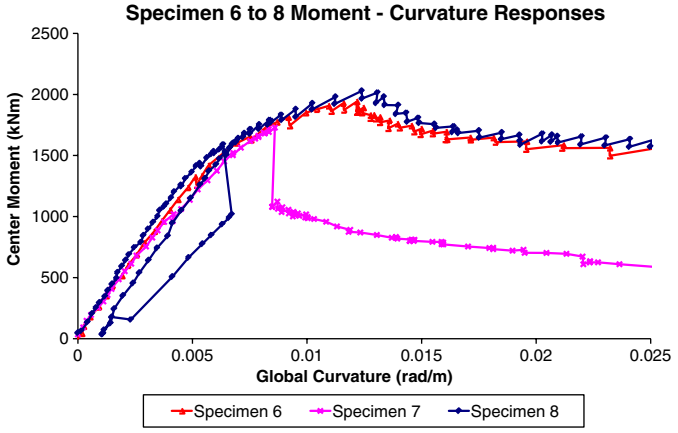

Fig. 9. Group 3 specimens moment-curvature responses

3 was greater than that of specimen 7. This illustrates that the moment capacity of an unpressurized cold bend is more influenced by its plastic section modulus than its material yield strength (Murray et al. 1992), because specimen 3 demonstrated a greater wall thickness, but a lower yield strength, than specimen 7.

Global Curvature at Maximum Moment

From Figs. 7–9, it is demonstrated that the specimens experienced several unloading cycles during testing. These were required for various reasons such as instrumentation repair, an end plate weld failure, and for end buckle prevention (Sen et al. 2005a). These unloading cycles did not compromise the validity of the experiments because there was very little plastic deformation in the specimens associated with reloading. The global curvature corresponding to the peak moment is used herein to assess the allowable global deformation prior to buckling of the specimens.

In Fig. 7, which compares the global behaviors of the Group 1 specimens, it is demonstrated that specimen 1 (the pressurized straight specimen) could undergo approximately 1.4 times the rotation between its ends prior to buckling than Specimen 2 (the pressurized cold bend specimen). It is also demonstrated in this figure that the pressurized cold bend specimen could undergo approximately 1.5 times the rotation between its ends prior to buckling than the unpressurized cold bend specimen.

For the Group 2 specimens, Fig. 8 demonstrates that specimen 5 experienced approximately 1.2 times the curvature prior to buckling compared to specimen 4. This is contrary to what would be expected because specimen 5 was bent at a greater kink angle

per interval than specimen 4, which would intuitively decrease the prebuckling deformability of the specimen. As the geometries and internal pressure for the two specimens were similar, possible explanations for the difference in curvature at buckling are the variation in material properties between the two pipes as they came from different heats of steel (Sen et al. 2005a), or differences in testing repeatability. In Fig. 8, the vertical line exhibited by specimen 5 was a result of the rotation meters not working, which required unloading and reloading of the specimen.

When Group 3 specimen behaviors are studied, it is demonstrated in Fig. 9 that the global curvature at peak moment for the unpressurized specimen 7 was approximately 0.75 times that for the pressurized specimens 6 and 8. Also, different kink angles per interval of specimens 6 and 8 did not significantly affect their global curvature at peak moment. These results verify the global behaviors of specimens 2 to 5, which will be summarized in the conclusion section of this paper. In Fig. 9, the vertical line exhibited by specimen 7 was a result of the rapid unloading of this specimen upon buckling. The vertical line exhibited by specimen 8 was a result of a rotation meter malfunction that occurred during the installation of a second set of end collars.

In comparing the global curvature at buckling for all of the pressurized specimens, generally the global curvature that corresponded to the peak moment was greatest for the Group 2 specimens, followed by the Group 1 specimens, and the Group 3 specimens generally demonstrated the lowest global curvature at the peak moment. This contradicts the findings in straight pipe research, where it is demonstrated that increasing internal pressure increased the allowable curvature at local buckling (Gresnigt et al. 1986); consequently, it may be inferred that the global curvature at buckling for the pressurized cold bends was more sensitive to D/t ratio and material grade as opposed to internal pressure. The global behavior for the unpressurized specimens contrasted these findings. That is, the global curvature at the peak moment for specimen 7 was greater than that of specimen 3, while specimen 7 demonstrated a higher D/t ratio than specimen 3. This demonstrates that the global behavior of unpressurized cold bends may be more sensitive to its material properties than to its D/t ratio.

Local Behavior

The compression side strain distribution along the pipe for the moments at which strain measurements over a 254 mm gauge length were recorded are demonstrated in Figs. 10 and 11. Specimens 2 and 3 herein are used to describe the local behaviors of all of the pressurized and unpressurized specimens, respectively. In these figures, the solid lines indicate the strain measurements that were taken prior to buckling, the heavy line indicates the strain measurement at the maximum moment, and the dashed lines represent the strain measurements recorded during postbuckling. The series order in the legends of Figs. 10 and 11 are organized from the first to the last recording of the strain measurements, thus the changes in strain distribution with respect to the load history of the tests is also illustrated in the plot. The origin of the horizontal axis corresponds to the middle of the specimen length, the origin of the vertical axis corresponds to zero strain, and the precise values for the vertical axis are available in (Sen et al. 2005b).

The first series in Fig. 10 corresponds to the pipe strains with internal pressure and zero jack load, and it is demonstrated that the internal pressure acting against the endplates forced the entire bottom of the pipe into tension. Furthermore this force induced the specimen into reverse curvature, as the tensile strains were greater at the ends of the pipe than at the middle. From the initiation of jack loading until an applied moment of 2,159 kNm, the strains primarily accumulated at the ends of the specimen. This showed

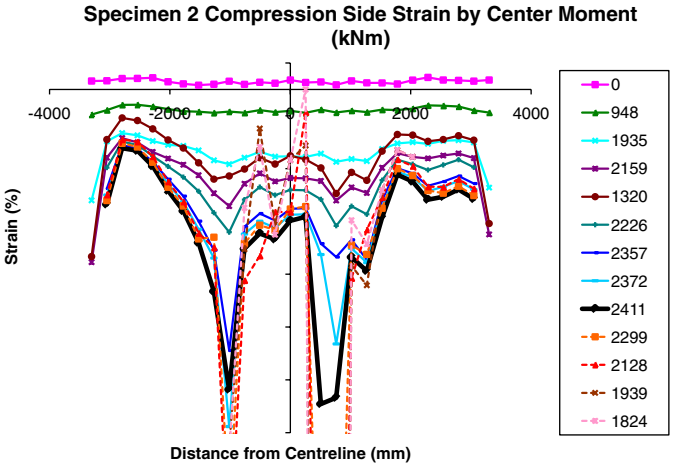

Fig. 10. Specimen 2 strain distribution by increasing load step

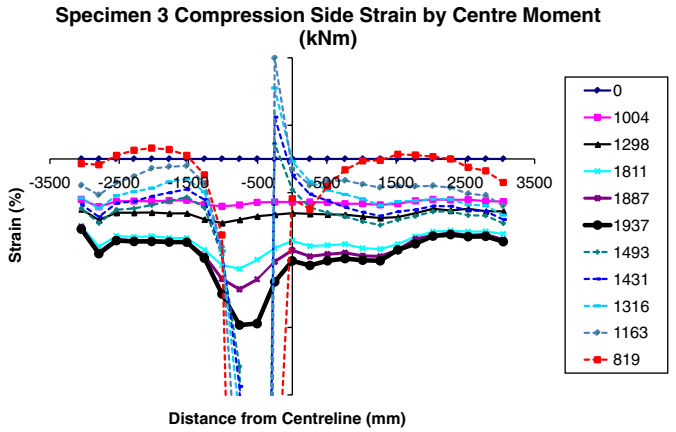

Fig. 11. Specimen 3 strain distribution by increasing load step

that an end buckle had formed at this location. Consequently, the specimen was unloaded, and a second set of collars was installed to confine the end buckle. Upon reloading, two 762 mm long bulges commenced to form at the—1,016 and 762 mm positions. The strain subsequently accumulated relatively equally at these two bulges until the maximum moment of 2,411 kNm was achieved. After the peak moment, the strains primarily accumulated at the buckle positioned at the 762 mm position. During postbuckling, strain relaxation occurred at the locations away from the buckle.

The strain distribution for specimen 3 shown in Fig. 11 demonstrates that the strains were relatively uniform throughout the specimen until an applied moment of 1,004 kNm, although the strains at the eventual buckle location were slightly higher than those at the other locations throughout testing. Closer observation indicates small increases in strain at the −2,794 and 1,240 mm locations, although these locations did not accumulate strains at higher rates than the other locations. After the moment of 1,004 kNm the strain at the −1,016 mm location were accumulating at slightly higher rates than those over the remainder of the specimen, and this trend continued until the maximum moment of 1,937 kNm was achieved. Immediately after the maximum moment was achieved the strain at the 1,016 mm position increased by seven fold, indicating there was a sudden collapse of the specimen. After buckling, tensile strains were observed to either side of the buckle. These strains are a result of the shape of the buckle and do not reflect on the global response of the pipe. The lack of numerous

bulges in the specimen, as exhibited in Fig. 10, and the sudden collapse after the peak moment was achieved, may be attributed to the absence of internal pressure, which tended to act as a stabilizing force for the cold bends.

Critical Strain

To assess the allowable compressive deformation prior to local buckling of the specimens, the critical strain of the specimens were measured during testing. This is the strain at the buckle location, over a gauge length of one diameter, which corresponded to the peak moment during testing. It was also desired to predict the critical strain of the specimens, to obtain a benchmark for comparison with the test results. Eq. (2) was selected for this undertaking, which is the critical strain predictive equation for a plain straight pipe with a rounded stress-strain curve (Dorey et al. 2001). This equation did not account for any of the effects from the cold bending of the pipes; however, the results will provide some idea of the expected critical strains for the specimens. It was assumed that there was an initial imperfection magnitude of 2% of the wall thickness for all of the specimens during the application of Eq. (2) herein.

$$\varepsilon_{\text{crit}} = \left(\frac{2.94}{D/t}\right)^{1.59} \cdot \left[\frac{1}{1 - 0.868\left(\frac{p}{p_y}\right)}\right] \cdot \left(\frac{E}{F_y}\right)^{0.854} \cdot \left[1.27 - \left(\frac{imp}{100}\right)^{0.150}\right] \quad (2)$$

where $\varepsilon_{\text{crit}}$ = critical strain over a gauge length of one diameter; t = wall thickness; D = diameter; E = modulus of elasticity; F_y = yield strength; imp = imperfection magnitude expressed as a percentage of the diameter; p = internal pressure; and p_y = internal pressure that causes the hoop stress in the pipe wall to achieve the yield stress.

The predicted and test critical strains are shown in Table 2. In this table, all of the test critical strains have been normalized against the specimen 1 test critical strain. This will allow for direct comparison of the cold bend to straight pipe critical strain, and comparisons of the critical strains between the cold bend specimens. The numerical values for the test critical strains are available in (Sen et al. 2005b).

Comparing the test critical strains of specimens 1 and 2 in Group 1 allows for interpretations concerning the overall effects of cold bending on the critical strain of a straight pipe. As shown in Table 2, the critical strain of specimen 1 was nearly two times that of specimen 2. This reduction in critical strain for the cold bend specimen occurred because of the changes in material properties, initial imperfections, and residual stresses that were introduced to the pipe during cold bending (Bilston et al. 1993). The critical strain of specimen 2 was 2.3 times that of specimen 3, which demonstrates that the presence of internal pressure substantially increased the critical strain of the cold bend. This behavior occurred because the internal pressure resisted the inward direction diamond mode buckling during loading, which forms at a lower applied energy level than that of the bulge mode buckle (Olsen et al. 1996).

When examining the critical strains of the Group 2 specimens in Table 2, the ratio of the specimen 4 critical strain compared with that of specimen 5 was 1.2. This ratio is relatively small, which shows that varying the kink angle per interval during the cold bending of these specimens did not significantly affect their critical strains (Behbahanifard et al. 2004).

The critical strain of the Group 3 specimen 7 is compared to that of specimen 8 because these two specimens were bent with similar kink angles per interval, and their materials were from the same heat of steel. The critical strain of specimen 8 was 4.3 times that of the specimen 7, which indicates that the stabilizing effect of the internal pressure becomes very dominant in the prebuckling behavior of the cold bends with high diameter to thickness ratios (Behbahanifard et al. 2004). The critical strain for specimen 8 was 1.3 times that of specimen 6, which is intuitively different than what would be expected because specimen 8 was bent more severely than specimen 6. However, this increase in critical strain is relatively minor, and may be explained by the different material properties of the specimens as they were formed from different heats of steel (Sen et al. 2005a).

The critical strain test to predicted ratios ranged from 0.43 to 0.85 for the cold bends (Sen et al. 2005b). Accordingly, the average test to predicted ratio for the cold bend specimens was 0.57. As Eq. (2) considerably overpredicted the critical strain for all of the cold bend specimens, but demonstrated a reasonable correlation with that of straight pipes (Dorey et al. 2001), perhaps the cold bending process significantly reduced the critical strain of the cold bend test specimens. Eq. (2) was derived based on a critical strain determination method that is different from the buckle strain at the peak moment, and is the method that was employed for this testing program (Dorey et al. 2001). Nonetheless, this equation may be employed herein, as it has reasonably predicted the critical strains for a large database of pipe tests regardless of the critical strain determination method.

Comparing the critical strains of the two unpressurized specimens reveals the effects of D/t ratio on the critical strain of the unpressurized cold bends. The critical strain of specimen 2 was 1.3 times that of specimen 7, while specimen 2 demonstrated a lower material specified minimum yield strength (SMYS). Because the two pipes were of the same diameter and had similar bending methods, but specimen 2 demonstrated a greater wall thickness, decreasing the diameter/thickness ratio for the unpressurized cold bends generated an increase in the critical strain.

Increasing internal pressure generally increased the critical strain of the cold bend specimens, similar to the behavior for straight pipes as demonstrated in Eq. (2). The normalized critical strain for specimen 2 was 0.51, the average normalized critical strain of specimens 4 and 5 was 0.56, and the average normalized critical strain of specimens 6 and 8 was 0.66. These are the average critical strains of the cold bends that demonstrated hoop stresses of 60, 40, and 80% of their respective SMYSs during testing. Thus, the average critical strain for specimens 6 and 8 was greater than the average for the other specimen groups, although they demonstrated the greatest diameter/thickness ratios while exhibiting similar material grades and bend geometries. Furthermore, the critical strain of specimen 2 was only slightly less than the average critical strain for specimens 4 and 5, although its D/t ratio was 50% larger and its material SMYS was 25% less than that of specimens 4 and 5, while the bend geometries were similar. Consequently, as specimen 2 was pressurized to 60% SMYS hoop stress while specimens 4 and 5 were pressurized to only 40% hoop stress, it is indicated that the internal pressure demonstrated a dominant role in the critical strain of these cold bends.

Conclusions

1. It has been demonstrated that cold bending played a significant role on the behavior of the specimens under applied bending. The maximum moment and corresponding curvature at the onset of buckling was decreased for the cold bend pipe in comparison to a similar straight pipe. The critical strain of the straight pipe was two times that of the cold bend pipe during

testing. The critical strain of all of the cold bend specimens ranged from between 0.43 to 0.85 of that of a similar straight pipe as predicted by equation, with an average test cold bend to predicted straight pipe ratio of 0.57.

2. In comparing the effects of varying the degree and interval length of the individual bends created during cold bending, the behaviors of specimens 4 and 5, and those of specimens 6 and 8, were compared with one another. For the pressurized specimens within each group, the moment curvature responses were very similar, and the strain distribution demonstrated moderately similar behaviors during the tests. The critical strains using the maximum moment method were similar for the equivalent specimens that were bent using different bending methods. Additionally, the postbuckling behavior was essentially the same for the equivalent specimens with different bending methods.
3. The unpressurized specimens buckled in a diamond shaped pattern while the pressurized specimens demonstrated a bulge buckle. The moment capacity of the unpressurized specimens decreased by 30% immediately after they buckled. In addition, the absence of internal pressure significantly decreases the peak moment capacity and critical strain of a cold bend pipe in comparison with a similar pipe that was pressurized. The critical strain of the unpressurized specimens was between 23 to 45% of a similar pressurized specimen. The postbuckling moment capacity of the unpressurized specimens was also considerably less than that of similar pressurized specimens.
4. Increasing the D/t ratio and internal pressure of the specimens corresponded to a decrease in peak moment capacity and global curvature at the onset of buckling. Increasing the internal pressure increased the magnitude of the bulges in the specimens prior to buckling. Finally, the postbuckling moment capacity to peak moment ratio increased with increasing D/t ratio and internal pressure.

Acknowledgments

This research project was conducted with the financial assistance from SNAM Rete Gas Ltd. and Tokyo Gas Ltd. In addition to their valuable financial contributions, several members of the industrial sponsor companies provided greatly appreciated technical assistance to this project. In particular, we would like to thank M. Como and E. Cerelli from SNAM Rete Gas Ltd., along with K. Yoshizaki and N. Fukada from Tokyo Gas Ltd. We would also like to acknowledge the technical assistance of K. Adams and S. Adeeb from TransCanada Pipelines Ltd., along with the much appreciated expertise of D.W. Murray from the University of Alberta.

Notation

The following symbols are used in this paper:

C = applied axial force;
C_y = axial load under zero circumferential stress;
D = pipe outside diameter;
E = modulus of elasticity;
F_y = yield strength;
imp = imperfection magnitude expressed as a percent of wall thickness;
Mp = plastic moment capacity;
p = internal pressure;
p_y = internal pressure that causes pipe wall to achieve the yield stress;
t = wall thickness;
Z = plastic section modulus;
ε_{crit} = critical strain over a gauge length of one diameter;
σ_y = yield stress; and
$\sigma\theta$ = circumferential stress.

References

ASME. (1999). "Process piping—ASME code for pressure piping." *B31.3-1999*, New York.

Beer, F. P., and Johnston, E. R. (1992). *Mechanics of materials—Second edition in SI units*, McGraw-Hill, New York.

Behbahanifard, M., et al. (2004). "Simulation of cold bends by finite element method." *Proc., 5th Biennial Int. Pipeline Conf.*, ASME, Calgary, Alberta, Canada, 427–435.

Bilston, P., and Murray, N. (1993). "The role of cold field bending in pipeline construction." *8th Symp. on Line Pipe Research*, American Gas Association, Washington, DC, 27.

Bouwkamp, G., and Stephen, R. M. (1973). "Large diameter pipe under combined loading." *Transp. Engrg. J.*, 99(TE3), 521–536.

Boyle, J. T., and Spence, J. (1981). "A simple stress analysis for out-of-round pressurized pipe bends." *Int. J. Pressure Vessels*, 9(4), 251–261.

Canadian Standards Association. (2003). "Z662-03 Oil and Gas Pipeline Systems." Etobicoke, Ontario, Canada.

Dorey, A. B., Cheng, J. J. R., and Murray, D. W. (2001). "Critical buckling strains for energy pipelines." *Structural Engineering Rep. No. 237*, Dept. of Civil Engineering, Univ. of Alberta, Edmonton, Alberta, Canada.

Fukada, N., Yatabe, H., Masuda, T., and Toyoda, M. (2002). "Changes in tensile properties due to cold bending of line pipes." *Proc., OMAE'02 21st Int. Conf. on Offshore Mechanics and Arctic Engineering*, ASME, New York.

Fukada, N., Yatabe, H., Watanabe, T., Kawaguchi, S., and Masuda, T. (2001). "Experimental and analytical study of cold bending process for pipelines." *Proc., OMAE'01 20th Int. Conf. on Offshore Mechanics and Arctic Engineering*, ASME, New York.

Gresnigt, A. M. (1986). "Plastic design of buried steel pipelines in settlement areas." *Heron*, 31(4), 1–113.

Mohareb, M. E., Elwi, A. E., Kulak, G. L., and Murray, D. W. (1994). "Deformational Behaviour of Line Pipe." *Structural Engineering Report No. 202*, Dept. of Civil Engineering, Univ. of Alberta, Edmonton, Alberta, Canada.

Murray, N. W., and Bilston, P. (1992). "Elasto-plastic and strain-hardening bending of thin steel pipes in the pre-buckling region." *Trans. Inst. Eng Aust. Civ. Eng.*, CE34(3), 247–253.

Olson, R., Clark, T., and Odom, T. (1996.) "Evaluation of the structural integrity of cold field bent line pipe." *9th Symp. on Pipeline Research*, Pipeline Research Council International (PRCI), Falls Church, VA.

Sen, M., Cheng, J. J. R., and Murray, D. W. (2005a). "Behaviour of cold bend pipes under combined loads." Ph.D. thesis, Dept. of Civil Engineering, Univ. of Alberta, Edmonton, Alberta, Canada.

Sen, M., Cheng, J. J. R., and Murray, D. W. (2005b). "Behaviour of cold bend pipes under combined loads." *Pipeline Technology Report 2005*, Dept. of Civil Engineering, Univ. of Alberta, Edmonton, Alberta, Canada.

Sen, M., Cheng, J. J. R., Murray, D. W., and Zhou, J. (2008). "Mechanical properties of cold bend pipes." *J. Pressure Vessel Technol.*, 130(2), 251–257.

Sen, M., et al. (2004). "Full scale tests of cold bend pipes." *Proc., 5th Biennial Int. Pipeline Conf.*, ASME, Calgary, Alberta, Canada, 419–426.